Lattice-Boltzmann models for high speed flows

Chenghai Sun
State Key Laboratory of Tribology, Department of Engineering Mechanics, Tsinghua University, Beijing 100084, China
(Received 17 December 1997; revised manuscript received 22 May 1998)

We formulate a lattice Boltzmann model to solve supersonic flows. The particle velocities are determined by the mean velocity and internal energy. The adaptive nature of particle velocities permits the mean flow to have a high Mach number. The introduction of a particle potential energy causes the model to be suitable for a perfect gas with an arbitrary specific heat ratio. The macroscopic conservation equations are derived by the Chapman-Enskog method. The simulations were carried out on the hexagonal lattice. However, the extension to both two- and three-dimensional square lattices is straightforward. As preliminary tests, we present the Sod shock-tube simulation and the two-dimensional shock reflection simulation. [S1063-651X(98)15911-1]

PACS number(s): 47.40.−x, 05.50.+q, 51.20.+d

I. INTRODUCTION

The lattice gas automaton (LGA) model was introduced as an alternative to traditional methods for numerically solving the Navier-Stokes equation [1]. The standard LGA models impose, for the sake of computational efficiency, a Boolean constraint that restricts the number of particles with a given velocity at a site to be zero or 1. The local equilibrium of the mean population of particles is described by the Fermi-Dirac statistics. Therefore, LGA models suffer from statistical noise and non-Galilean invariance. These difficulties have led to the development of lattice Boltzmann (LB) models [2,3]. In the lattice Boltzmann method, space and time are discrete as they are in the LGA method. Instead of using a bit representation for particles, real numbers represent the local ensemble-averaged particle distribution functions, and only kinetic equations for the distribution functions are solved. The LB method ignores particle-particle correlation and often uses the simple Bhatnagar-Gross-Krook collision operator. However, even under these simplifications they provide the correct evolution of the macroscopic quantities. The LB method has considerable flexibility in the choice of the local equilibrium particle distribution. By this additional freedom, the desired physical properties, such as Galilean invariant convection, can be achieved. Readers are referred to a recent review article [4] for a variety of LB models.

In the LB method, as well as in the LGA method, the particle velocities belong to a finite set. Consequently, the macroscopic velocity is limited. In general, the LB method suffers from the restraint of a small Mach number. Alexander, Chen, and Doolen [5] attempted to decrease the sound speed to augment the Mach number. Moreover, Burger's equation was simulated, showing reasonable agreement compared to the exact solution. Qian and Orszag [6] studied the nonlinear deviation of the LB model in a compressible regime, and presented a numerical simulation of a shock profile. Recently, the gas-kinetic theory [7,8] and the discrete-velocity model [9] successfully simulated the compressible Euler equation. The finite volume method was employed to solve the Boltzmann equations. The discontinuities were well captured. Reference [10] proposed a compressible LB model and successfully simulated the Sod shock-tube problem. However, due to the restraint mentioned above, the standard LB method has great difficulty in simulating compressible Euler flows at a high Mach number. In the present paper, we propose a locally adaptive LB model. The particle velocity set is chosen according to the fluid local velocity and internal energy, which no longer limits the fluid velocity. Consequently, the model is suitable for a wide range of Mach numbers. The specific heat ratio γ can be adjusted freely by introducing the particle potential energy. In Sec. II we first present an LB model with a discrete particle velocity and continuous momentum and kinetic energy, and then derive the corresponding general macroscopic conservation equations by the Chapman-Enskog method. In Sec. III we determine the equilibrium distribution for supersonic flows. Then the macroscopic conservation equations are turned to be the Navier-Stokes equations. Section IV is about the simulation. Section V is the conclusions.

II. SEMIDISCRETE VELOCITY LB MODEL

In the standard LB model, space, time, and the particle velocity are all discrete. The particle with velocity $\mathbf{c}$ has the momentum $m\mathbf{c}$ and kinetic energy $\frac{1}{2}m\mathbf{c}^2$, and moves a distance $\mathbf{c}$ from a node to another node during one step time, where m is the particle mass. Now we consider what we call a ''semidiscrete velocity LB model'': the particle velocity is discrete, while the momentum and kinetic energy may be continuous. We suppose that a particle has two velocities: the ''migrating velocity'' $\mathbf{r}$, transporting the particle from a node to its neighbor node at a distance $\mathbf{r}\Delta t$ during the discrete time Δt, and the velocity $\boldsymbol{\xi}\in\mathcal{D}$ for calculating the momentum and the kinetic energy of the particle, where $\mathcal{D}$ is a bounded domain in $\mathbb{R}^3$ (or in $\mathbb{R}^2$ for two-dimensional models) and $\mathbf{r}\in\mathcal{D}$. In other words, a particle with the migrating velocity $\mathbf{r}$ may have the momentum $m\boldsymbol{\xi}$ and kinetic energy $\frac{1}{2}m\xi^2$, where $\mathbf{r}$ is discrete and $\boldsymbol{\xi}$ is continuous. The objective of introducing such a semidiscrete velocity LB model is to increase the accuracy of the model. When the domain $\mathcal{D}$ constricts to $\mathbf{r}$, the semidiscrete model becomes the discrete model.

Let x be an arbitrary node of a lattice; $f(x,\mathbf{r},\boldsymbol{\xi},t)$ is the density distribution function for the particle with the velocity $\boldsymbol{\xi}$ and the migrating velocity $\mathbf{r}$, moving to $x+\mathbf{r}\Delta t$ during Δt. In order to obtain an arbitrary special heat ratio γ, we introduce the particle potential energy Φ [11]. The total energy of

a particle is the sum of kinetic energy and the potential energy, i.e., $\frac{1}{2}m\xi^2+m\Phi$. The conserved total mass, momentum and energy are defined as

$$\rho=\sum_{\mathbf{r}}\int_{\mathcal{D}} m f(x,\mathbf{r},\boldsymbol{\xi},t)d\boldsymbol{\xi}, \tag{1}$$

$$\rho\mathbf{v}=\sum_{\mathbf{r}}\int_{\mathcal{D}} m\boldsymbol{\xi} f(x,\mathbf{r},\boldsymbol{\xi},t)d\boldsymbol{\xi}, \tag{2}$$

$$\rho E=\sum_{\mathbf{r}}\int_{\mathcal{D}} m\left(\frac{1}{2}\xi^2+\Phi\right)f(x,\mathbf{r},\boldsymbol{\xi},t)d\boldsymbol{\xi}. \tag{3}$$

Define

$$\langle\cdot\rangle=\sum_{\mathbf{r}}\int_{\mathcal{D}}\cdot\, d\boldsymbol{\xi},$$

$$\boldsymbol{\eta}=\left(m,m\boldsymbol{\xi},m\left(\frac{1}{2}\xi^2+\Phi\right)\right)^T,$$

$$\mathbf{Y}=(\rho,\rho\mathbf{v},\rho E)^T.$$

Formulas (1), (2), and (3) can be written in the compact form

$$\mathbf{Y}=\langle\boldsymbol{\eta} f(x,\mathbf{r},\boldsymbol{\xi},t)\rangle. \tag{4}$$

In LB models, the Boltzmann equation is written as

$$f(x+\mathbf{r}\Delta t,\mathbf{r},\boldsymbol{\xi},t+\Delta t)-f(x,\mathbf{r},\boldsymbol{\xi},t)=\Omega, \tag{5}$$

where

$$\Omega=-\frac{1}{\tau}[f(x,\mathbf{r},\boldsymbol{\xi},t)-f^{\mathrm{eq}}(x,\mathbf{r},\boldsymbol{\xi},t)], \tag{6}$$

and $f^{\mathrm{eq}}(x,\mathbf{r},\boldsymbol{\xi},t)$ is the equilibrium distribution depending on the total mass, momentum, and energy.

Now we study the convective and the dissipative properties of the model from the Chapman-Enskog expansion of the solution of Eq. (5) [12]. We choose $\Delta t=\epsilon T$, where T is a reference time scale and ϵ a typical small parameter. We are then looking for a solution of Eq. (5) as an asymptotic expansion of the forms

$$f=\sum_{n=0}^{\infty}\epsilon^n f^{(n)}, \tag{7}$$

$$\frac{\partial\mathbf{Y}}{\partial t}=\sum_{n=0}^{\infty}\epsilon^n\mathbf{F}^{(n)}, \tag{8}$$

where $f^{(n)}$ and $\mathbf{F}^{(n)}$ depend only on $\mathbf{Y}$ and its successive gradients. $f^{(0)}=f^{\mathrm{eq}}$ is completely determined by the macroscopic variables ρ, $\rho\mathbf{v}$, and ρE, and verifies

$$\mathbf{Y}=\langle\boldsymbol{\eta} f^{\mathrm{eq}}(x,\mathbf{r},\boldsymbol{\xi},t)\rangle. \tag{9}$$

Considering the relations (4), (9), (7), and (6), we have

$$\langle\boldsymbol{\eta} f^{(n)}\rangle=\mathbf{0},\quad \forall\ n\geqslant 1 \tag{10}$$

$$\langle\boldsymbol{\eta}\Omega\rangle=\mathbf{0}. \tag{11}$$

We Taylor expand the left-hand side of Eq. (5):

$$\begin{aligned}\Delta f&=f(x+\mathbf{r}\Delta t,\mathbf{r},\boldsymbol{\xi},t+\Delta t)-f(x,\mathbf{r},\boldsymbol{\xi},t)\\&=\epsilon T\left\{\frac{\partial f^{(0)}}{\partial\mathbf{Y}}\cdot\mathbf{F}^{(0)}+\mathbf{r}\cdot\nabla f^{(0)}\right\}\\&\quad+\epsilon^2T\left\{\frac{\partial f^{(0)}}{\partial\mathbf{Y}}\cdot\mathbf{F}^{(1)}+\frac{\partial f^{(1)}}{\partial\mathbf{Y}}\cdot\mathbf{F}^{(0)}\right.\\&\quad\left.+\frac{\partial f^{(1)}}{\partial\nabla\mathbf{Y}}\cdot\nabla\mathbf{F}^{(0)}+\mathbf{r}\cdot\nabla f^{(1)}\right\}\\&\quad+\frac{\epsilon^2T^2}{2}\left\{\frac{\partial^2 f^{(0)}}{\partial\mathbf{Y}\partial\mathbf{Y}}:\mathbf{F}^{(0)}\mathbf{F}^{(0)}+\mathbf{rr}:\nabla\nabla f^{(0)}\right.\\&\quad\left.+2\mathbf{r}\cdot\left(\frac{\partial f^{(0)}}{\partial\mathbf{Y}}\cdot\mathbf{F}^{(0)}\right)+\frac{\partial f^{(0)}}{\partial\mathbf{Y}}\cdot\frac{\partial\mathbf{F}^{(0)}}{\partial t}\right\}.\end{aligned} \tag{12}$$

By identifying the first order terms of ϵ in Eq. (5), we can determine $f^{(1)}$, and, considering Eqs. (10) and (11), we obtain $\mathbf{F}^{(0)}$ and $\mathbf{F}^{(1)}$:

$$f^{(1)}=-\tau T\left\{\nabla f^{\mathrm{eq}}\cdot\mathbf{r}+\frac{\partial f^{\mathrm{eq}}}{\partial\mathbf{Y}}\cdot\mathbf{F}^{(0)}\right\},$$

$$\mathbf{F}^{(0)}=-\operatorname{div}\langle\mathbf{r}f^{\mathrm{eq}}\boldsymbol{\eta}\rangle,$$

$$\mathbf{F}^{(1)}=-\operatorname{div}\left\langle\left\{f^{(1)}\mathbf{r}+\frac{T}{2}\left[\operatorname{div}(f^{\mathrm{eq}}\mathbf{rr})+\frac{\partial f^{\mathrm{eq}}}{\partial\mathbf{Y}}\cdot\mathbf{F}^{(0)}\mathbf{r}\right]\right\}\boldsymbol{\eta}\right\rangle.$$

Up to order 1, Eq. (8) is written as

$$\begin{aligned}\frac{\partial\mathbf{Y}}{\partial t}&=-\operatorname{div}\langle f^{\mathrm{eq}}\mathbf{r}\boldsymbol{\eta}\rangle-\epsilon T\left(\frac{1}{2}-\tau\right)\operatorname{div}\left[\operatorname{div}\langle f^{\mathrm{eq}}\mathbf{rr}\boldsymbol{\eta}\rangle\right.\\&\quad\left.+\left\langle\frac{\partial f^{\mathrm{eq}}}{\partial\mathbf{Y}}\cdot\mathbf{F}^{(0)}\mathbf{r}\boldsymbol{\eta}\right\rangle\right].\end{aligned} \tag{13}$$

This macroscopic conservation equation depends on the distribution of f^{eq}. In Sec. III we will see that if the equilibrium distribution is properly determined it may become the Navier-Stokes equation.

III. EQUILIBRIUM DISTRIBUTIONS

We consider the symmetric vector set $\{\mathbf{c}'_{j\nu};j=1,\ldots,b_\nu\}$ connecting a node to its equal distance neighbor nodes on a regular lattice, where b_ν is the number of vector directions. For a hexagonal lattice we choose $b_\nu=6$. $\nu=1$ and 2. The module of $\mathbf{c}'_{j\nu}$ is c'_ν. Let x be an arbitrary node; $\mathbf{v}$ is the fluid velocity at this node, and $\mathbf{v}_1$, $\mathbf{v}_2$, and $\mathbf{v}_3$ are the vectors from the node x to the apexes of the triangle containing the velocity vector $\mathbf{v}$. We introduce the particle velocities $\mathbf{c}_{j\nu k}$ and $\overline{\mathbf{c}}_{j\nu}$ and the fluctuating velocities $\mathbf{v}'_k$ $(k=1,2,3)$:

$$\mathbf{c}_{j\nu k}=\mathbf{v}_k+\mathbf{c}'_{j\nu}, \tag{14}$$

$$\overline{\mathbf{c}}_{j\nu}=\mathbf{v}+\mathbf{c}'_{j\nu}, \tag{15}$$

$$\mathbf{v}_k=\mathbf{v}+\mathbf{v}'_k. \tag{16}$$

In the standard LB models, the particle velocities are constant; therefore, the mean velocity (i.e., the fluid velocity) is limited. In present model, the particle velocities are adapted to the mean velocity. The mean velocity is then rid of the constraint of the particle velocities. For high speed flow the fluctuating velocities $\mathbf{v}'_k$ is small.

For $\mathbf{r}=\mathbf{c}_{j\nu k}$, we define

$$f^{\mathrm{eq}}_{j\nu k}(x,\boldsymbol{\xi},t)=f^{\mathrm{eq}}(x,\mathbf{c}_{j\nu k},\boldsymbol{\xi},t),$$

and for the other $\mathbf{r}$ we set $f^{\mathrm{eq}}(x,\mathbf{r},\boldsymbol{\xi},t)=0$. We suppose $f^{\mathrm{eq}}_{j\nu k}(x,\boldsymbol{\xi},t)$ to have the form

$$f^{\mathrm{eq}}_{j\nu k}(x,\boldsymbol{\xi},t)=d_{\nu k}\delta(\boldsymbol{\xi}-\overline{\mathbf{c}}_{j\nu}), \tag{17}$$

where $\delta(\boldsymbol{\xi})$ is the δ function. $\delta(\boldsymbol{\xi})=0$ for $\boldsymbol{\xi}\neq\mathbf{0}$; $\int g(\boldsymbol{\xi})\delta(\boldsymbol{\xi})d\boldsymbol{\xi}=g(\mathbf{0})$. Equation (13) becomes

$$\frac{\partial\mathbf{Y}}{\partial t}=-\operatorname{div}\sum_{k,\nu,j}\left\{d_{\nu k}\mathbf{c}_{j\nu k}\boldsymbol{\eta}_{j\nu}+\alpha\left[\operatorname{div}(d_{\nu k}\mathbf{c}_{j\nu k}\mathbf{c}_{j\nu k}\boldsymbol{\eta}_{j\nu})+\mathbf{F}^{(0)}\cdot\frac{\partial}{\partial\mathbf{Y}}(d_{\nu k}\mathbf{c}_{j\nu k}\boldsymbol{\eta}_{j\nu})\right]\right\}, \tag{18}$$

where $\alpha=\epsilon T(\frac{1}{2}-\tau)$, and

$$\boldsymbol{\eta}_{j\nu}=(m,m\overline{\mathbf{c}}_{j\nu},m(\tfrac{1}{2}\overline{\mathbf{c}}^2_{j\nu}+\Phi))^T. \tag{19}$$

Substituting $f^{\mathrm{eq}}_{j\nu k}$ into Eq. (9), we have

$$\rho=\sum_{k,\nu}mb_\nu d_{\nu k}=\sum_{k=1}^{3}\rho_k, \tag{20}$$

$$\rho E=\sum_{k,\nu,j}md_{\nu k}[\tfrac{1}{2}(\mathbf{v}+\mathbf{c}'_{j\nu})^2+\Phi]$$

$$=\tfrac{1}{2}\rho\mathbf{v}^2+\sum_{k,\nu}\tfrac{1}{2}mb_\nu d_{\nu k}c'^2_\nu+\rho\Phi, \tag{21}$$

where $\rho_k=\Sigma_\nu mb_\nu d_{\nu k}$. The second component of Eq. (9) is automatically verified as long as $d_{\nu k}$ verify Eq. (20). In order to increase the accuracy, we assume that ρ_k satisfy the following equation:

$$\rho\mathbf{v}=\sum_{k=1}^{3}\rho_k\mathbf{v}_k. \tag{22}$$

For a given ρ and $\rho\mathbf{v}$ it can be proved that Eqs. (20) and (22) have unique non-negative solutions for ρ_k (see Fig. 1).

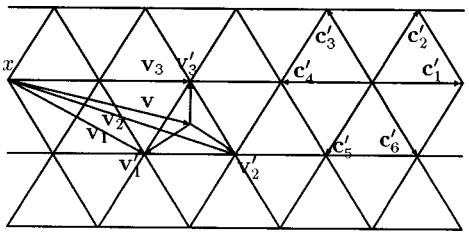

FIG. 1. Particle velocities.

Equations (20) and (22) permit us to write

$$\sum_k\rho_k\mathbf{v}'_k=\mathbf{0}. \tag{23}$$

Thanks to Eq. (23), we will see that the first order of $\mathbf{v}'_k$ in the conservation equations will disappear. We introduce the density portion $\alpha_k=\rho_k/\rho$, and we suppose $d_{\nu k}$ to have the form

$$d_{\nu k}=\alpha_k d_\nu, \tag{24}$$

where $d_\nu=\Sigma_k d_{\nu k}$ will be determined by the density and the pressure (or internal energy).

The perfect gas with special heat ratio γ verifies $p=(\gamma-1)\rho e$, where $e=E-\frac{1}{2}v^2$ is the internal energy. The pressure p has the form

$$p=\sum_\nu mb_\nu d_\nu\frac{1}{D}c'^2_\nu, \tag{25}$$

where D is the space dimension.

In the case where c'_ν have two levels ($\nu=1$ and 2), one can determine d_1, d_2, and Φ by Eqs. (20), (21), and (25):

$$d_1=\frac{\rho c'^2_2-Dp}{b_1m(c'^2_2-c'^2_1)},$$

$$d_2=\frac{Dp-\rho c'^2_1}{b_2m(c'^2_2-c'^2_1)},$$

$$\Phi=\left[1-\frac{D}{2}(\gamma-1)\right]e.$$

In order to ensure the positivity of d_1 and d_2, c'_1 and c'_2 are required to verify $c'^2_1<Dp/\rho<c'^2_2$. However, c'_1 and c'_2 are not completely determined. In practice, we choose c'_1 and c'_2 to be as close as possible to each other. For a two-dimensional Boltzmann model without particle potential energy, the special heat ratio γ is 2 [9]. From the relation above we can see that $\Phi=0$ when $\gamma=2$, agreeing with the standard LB models.

Now the equilibrium is completely determined. Considering relations (14), (15), (16), (22), and (23), we derive the continuity, momentum, and energy equations from Eq. (18):

$$\frac{\partial\rho}{\partial t}+\operatorname{div}(\rho\mathbf{v})=0, \tag{26}$$

$$\frac{\partial\rho\mathbf{v}}{\partial t}+\operatorname{div}(\rho\mathbf{v}\mathbf{v})+\nabla p=\operatorname{div}\{\mu[\nabla\mathbf{v}+(\nabla\mathbf{v})^T-(\gamma-1)\operatorname{div}\mathbf{v}\mathbf{I}_d]+B_1\}, \tag{27}$$

$$\rho\frac{\partial E}{\partial t}+\operatorname{div}(p\mathbf{v}+\rho E\mathbf{v})=\operatorname{div}\{\mu\mathbf{v}\cdot[\nabla\mathbf{v}+(\nabla\mathbf{v})^T-(\gamma-1)\operatorname{div}\mathbf{v}\mathbf{I}_d]\}+\epsilon T(\tau-\tfrac{1}{2})\operatorname{div}\{\nabla A+\nabla(p\Phi)-\gamma e\nabla p+B_2\}, \tag{28}$$

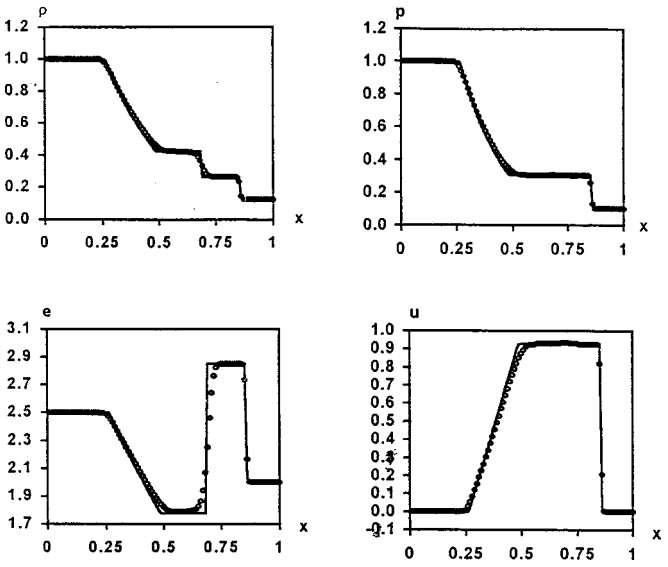

FIG. 2. The sod shock-tube problem: the profiles of density, pressure, internal energy, and velocity at the 80th iteration time on a 400×4 node lattice ($\tau=1$ and $\gamma=1.4$). The solid lines are the exact solutions of the Euler system.

where

$$\mu=\epsilon T(\tau-\tfrac{1}{2})p,$$

$$B_1=\mathrm{div}\sum_{k,\nu} mb_\nu d_{\nu k}\mathbf{v}\mathbf{v}'_k\mathbf{v}'_k,$$

$$B_2=\mathrm{div}\sum_{k,\nu} mb_\nu d_{\nu k}[\tfrac{1}{2}(v^2+c'^2_\nu)+\Phi]\mathbf{v}'_k\mathbf{v}'_k,$$

$$A=\sum_\nu mb_\nu d_\nu \frac{1}{2D}c'^4_\nu.$$

ϵT is the time step, and μ is the viscosity. In Eq. (28) the first and the second terms on the right-hand side correspond, respectively, to the dissipation and the diffusion. B_1 and B_2 can be regarded as discretion error. Then Eqs. (26), (27), and (28) become Navier-Stokes equations.

In the discrete velocity LB model case, the distribution of f^{eq} in phase space of $\boldsymbol{\xi}$ concentrates at $\mathbf{c}_{j\nu k}$, i.e.,

$$f^{\mathrm{eq}}_{j\nu k}(x,\boldsymbol{\xi},t)=d_{\nu k}\delta(\boldsymbol{\xi}-\mathbf{c}_{j\nu k}),$$

and $\boldsymbol{\eta}_{j\nu}$ in Eq. (18) is replaced by

$$\boldsymbol{\eta}_{j\nu k}=(m,m\mathbf{c}_{j\nu k},m(\tfrac{1}{2}\mathbf{c}^2_{j\nu k}+\Phi))^T. \tag{29}$$

Then, from Eq. (18) we obtain the continuity equation (26) and momentum and energy equations similar to Eqs. (27) and (28). But there are additional terms $\mathrm{div}\Sigma_{k,\nu}mb_\nu d_{\nu k}\mathbf{v}'_k\mathbf{v}'_k$ and $\mathrm{div}\Sigma_{k,\nu}mb_\nu d_{\nu k}\frac{1}{2}v'^2_k\mathbf{v}$ on the left-hand sides of the momentum and energy equations, respectively. Therefore, this model is less accurate. This is the reason that we have established the present semidiscrete velocity LB model.

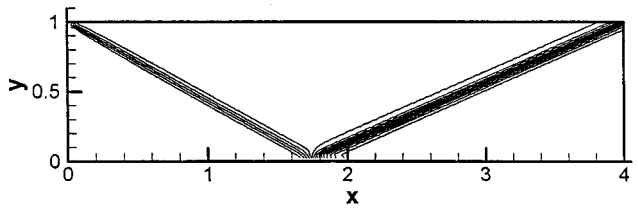

FIG. 3. Shock reflection: pressure contours at the 600th iteration; grid size: 280×80. Left and up boundary conditions: $(\rho,u,v,p)|_{(0,y,t)}=(1.0,2.9,0.0,1/1.4)$; $(\rho,u,v,p)|_{(x,1,t)}=(1.69997, 2.1934,-0.50633,1.52819)$.

IV. NUMERICAL SIMULATIONS

If we regard the viscous terms and the diffusion terms of the right-hand sides of Eqs. (27), and (28) as the discretion error, Eqs. (26), (27), and (28) become an inviscid Euler system. In fact, the viscosity and diffusivity are of order $(\tau-\frac{1}{2})l^2/\Delta t$, where l is the unit length of the lattice and $\Delta t(=\epsilon T)$ is the unit time. The model is of first order for the Euler system, and second order for the Navier-Stokes system.

When $\tau=1$ the Boltzmann equation (5) becomes

$$f_{j\nu k}(x+\mathbf{c}_{j\nu k}\Delta t,t+\Delta t)=f^{\mathrm{eq}}_{j\nu k}(x,t).$$

Since $f^{\mathrm{eq}}_{j\nu k}$ depends only on fluid density, velocity, and internal energy, the particle distribution $f_{j\nu k}$ at $t+\Delta t$ is also determined by them, independent of the particle distribution at time t. The need of computer memory and computation time is considerably reduced. We have performed the Sod test and the shock reflection simulation under the condition $\tau=1$ and $\gamma=1.4$.

A. Sod test

The classical Sod test [13] case is the blast-wave test with the initial conditions $\rho_l=1$, $p_l=1$, and $u_l=0;\rho_r=0.125$, $p_r=0.1$, and $u_r=0$ correspond to an initial pressure ratio of 10 and a density ratio of 8. Subscript l denotes the left half, and subscript r denotes the right half at time 0. The simulation was performed on a 400×4 node lattice. The periodical condition was taken in the y direction. Figure 2 shows the density, pressure, velocity, and internal energy profiles obtained from the present LB model simulation, where t is the 80th iteration. The solid lines in the figure represent the exact solution of the Euler system.

B. Shock reflection

The computational domain is a rectangle of length 4 and height 1 divided into 280×80 nodes. The Dirichlet conditions

$$(\rho,u,v,p)|_{(0,y,t)}=(1.0,2.9,0.0,1/1.4),$$

$$(\rho,u,v,p)|_{(x,1,t)}=(1.699\,97,2.193\,4,-0.506\,33,1.528\,19)$$

are imposed on the left and upper boundaries, respectively. The bottom boundary is a reflecting wall. Initially, the solution of the entire domain is set to be that at the left boundary [14]. Figure 3 shows the pressure contours. Figure 4 shows the corresponding pressure profile at $y=0.5$.

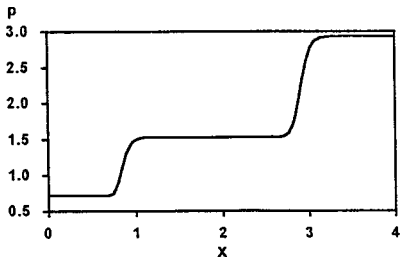

FIG. 4. p at $y=0.5$.

The simulations were carried out on Pentium II 266 personal computer. One time step needs 1.5 s on a 280×80 hexagonal lattice, i.e., about 6.7×10^{-5} s per node. The total time is proportional to the total number of nodes.

V. CONCLUSION

In this paper, we have established an LB model for high-speed flows. It can handle flows over a wide range of Mach numbers and capture shock jumps. The adaptive nature of the particle velocities makes a link between the LB model and the discrete-velocity models [15]. The courant model is of first order for Euler system and second order for Navier-Stokes system. We have performed the Sod shock-tube simulation and the two-dimensional shock reflection simulation. Although the simulations were carried out on a hexagonal lattice, the model can be easily applied to both two- and three-dimensional square lattices. Due to the simple form of the equilibrium distribution, the fourth-order velocity tensors do not involve in the calculations. On square lattices, there will be no need of a special treatment for the homogeneity of the fourth-order velocity tensors. The major limitation of the current model is that τ should be set to 1; otherwise, the simulations would need an enormous amount of computer memory and time.

ACKNOWLEDGMENT

This work was supported by the National Natural Science Foundation of China (Grant No. 19672030).

[1] U. Frisch, B. Hasslacher, and Y. Pomeau, Phys. Rev. Lett. **56**, 1505 (1986).
[2] H. Chen, S. Chen, and W. Matthaeus, Phys. Rev. A **45**, R5339 (1992).
[3] Y. H. Qian, D. d'Humières, and P. Lallemand, Europhys. Lett. **17**, 479 (1992).
[4] S. Chen and G. D. Doolen, Annu. Rev. Fluid Mech. **30**, 329 (1998).
[5] F. J. Alexander, H. Chen, and G. D. Doolen, Phys. Rev. A **46**, 1967 (1992).
[6] Y. H. Qian and S. A. Orszag, Europhys. Lett. **21**, 255 (1993).
[7] K. Xu, J. Stat. Phys. **81**, 147 (1995).
[8] K. Xu, L. Martinelli, and A. Jameson, J. Comput. Phys. **120**, 48 (1995).
[9] B. T. Nadiga, J. Stat. Phys. **81**, 129 (1995).
[10] S. X. Hu, G. W. Yan, and W. P. Shi, Acta Mech. Sin. **13**, 314 (1997).
[11] C. H. Sun, Z. J. Xu, B. G. Wang, and M. Y. Shen, Commun. Nonlinear Sci Numer. Simul. **2**, 212 (1997).
[12] D. Bernardin, O. Sero-Guillaume, and C. H. Sun, Physica D **47**, 169 (1991).
[13] G. A. Sod, J. Comput. Phys. **27**, 1 (1978).
[14] P. Colella, J. Comput. Phys. **87**, 171 (1990).
[15] R. Gatignol, *Lecture Notes in Physics* (Springer-Verlag, Berlin, 1975), Vol. 36.